Journal of Inorganic Biochemistry 232 (2022) 111812

Contents lists available at ScienceDirect

Journal of Inorganic Biochemistry

journal homepage: www.elsevier.com/locate/jinorgbio

A novel adenine-based diruthenium(III) complex: Synthesis, crystal structure, electrochemical properties and evaluation of the anticancer activity

Marta Orts-Arroyo [a], Fernanda Gutiérrez [b,c], Anabel Gil-Tebar [b,c], Maider Ibarrola-Villava [b,c], Elena Jiménez-Martí [b,c,d], Adriana Silvestre-Llora [a], Isabel Castro [a], Gloria Ribas [b,*], José Martínez-Lillo [a,*]

[a] Departament de Química Inorgànica, Instituto de Ciencia Molecular (ICMol), Universitat de València, 46980 Paterna, València, Spain
[b] Department of Medical Oncology, INCLIVA Biomedical Research Institute, Universitat de València, 46010 València, Spain
[c] CIBERONC, Centro de Investigación Biomédica en Red Cáncer, Instituto de Salud Carlos III, Spain
[d] Departament de Bioquímica i Biologia Molecular, Facultat de Medicina, Universitat de València, Spain

ARTICLE INFO

Keywords:
Ruthenium(III)
Adenine
Crystal structure
Cyclic voltammetry
Cancer cell lines
Cell viability

ABSTRACT

Metal complexes based on purine nucleobases can be a very useful tool in the diagnosis and treatment of some diseases as well as in other biomedical applications. We have prepared and characterized a novel dinuclear ruthenium(III) complex based on the nucleobase adenine of formula $[\{Ru(\mu\text{-}Cl)(\mu\text{-}Hade)\}_2Cl_4]Cl_2{\cdot}2H_2O$ (**1**) [Hade = protonated adenine]. Complex **1** was characterized through Fourier transform infrared spectroscopy (FT–IR), scanning electron microscopy and energy dispersive X-ray analysis (SEM–EDX), magnetometer (SQUID) and cyclic voltammetry (CV) techniques. The crystal structure of **1** was determined by single-crystal X-ray diffraction. **1** crystallizes in the monoclinic system with space group $P2_1/n$. Each ruthenium(III) ion is six-coordinate and bonded to four Cl atoms [the average value of the Ru^{III}-Cl bonds lengths is ca. 2.329(1) Å] and two N atoms (N3 and N9) from two adenine molecules, the N1 atom being protonated in both of them. The anticancer activity was evaluated through cell viability assays performed on a colon cancer (HCT116) and a gastric cancer cell lines (AGS), **1** showing an incipient anticancer effect on the AGS cell line at the highest concentration used in the study.

1. Introduction

Ruthenium coordination chemistry has undergone a considerable development in different research fields during the last two decades [1], including promising systems for current and future investigations that involve several oxidation states, which display a wide variety of technological applications covering from catalysis to anticancer drugs [2–11].

Heteroleptic mononuclear Ru^{III} complexes have proven to be particularly important for the design of metallic systems with exciting biological properties [12]. Some examples are the Ru^{III} complexes based on imidazole and indazole ligands [13,14], namely, the anionic complexes trans-[tetrachloro(dimethyl sulfoxide)(imidazole)ruthenate(III)] (NAMI-A) and trans-[tetrachlorobis(indazole)ruthenate(III)] (KP1019), which behave as anticancer and antimetastatic agents that have entered clinical trials [15–17].

In the literature, there exist a few ruthenium complexes based on nucleobases with tested antitumor activity [18–21], as for instance, the

Abbreviations: FT–IR, fourier transform infrared spectroscopy; SEM–EDX, scanning electron microscopy and energy dispersive X-ray analysis; CV, cyclic voltammetry; HCT116, colon cancer cell line; AGS, gastric cancer cell line; NAMI-A, *trans*-[tetrachloro(dimethyl sulfoxide)(imidazole)ruthenate(III)]; KP1019, *trans*-[tetrachlorobis(indazole)ruthenate(III)]; DMSO, dimethyl sulfoxide; PTA, 1,3,5-triaza-7-phosphaadamantane; 5′-AMP, adenosine 5′-monophosphate; MPMS, magnetic properties measurement system; SQUID, superconducting quantum interference device; DMF, N,N′-dimethylformamide; Fc, ferrocene; CCDC, cambridge crystallographic data centre; MTT, 3-(4,5-dimethylthiazolyl-2)-2,5-diphenyltetrazolium bromide; PI, propidium iodide; PBS, phosphate buffered saline; FITC, fluorescein isothiocyanate; PXRD, powder X-ray diffraction.

* Corresponding authors.
E-mail address: f.jose.martinez@uv.es (J. Martínez-Lillo).

https://doi.org/10.1016/j.jinorgbio.2022.111812
Received 11 January 2022; Received in revised form 10 March 2022; Accepted 31 March 2022
Available online 6 April 2022

thymine-based Ru^{II} complex $[Ru(PPh_3)_2(thy)(bpy)]PF_6$ [where PPh_3 = triphenylphosphine, thy = thymine and bpy = 2,2′-bipyridine], which is a potent cytotoxic agent that by DNA-binding induces apoptotic cell death in human colon carcinoma [18,19]. The first guanine-containing Ru^{III} complex of formula trans-$[Ru^{III}Cl_4(Hgua)(DMSO)]\cdot 2H_2O$ (Hgua = monoprotonated guanine) was reported in 2004 [20]. This compound was characterized by single-crystal X-ray diffraction and its in vitro antitumor activity was also evaluated, showing a mild antiproliferative effect but an interesting proadhesive effect [20]. With deprotonated adenine, the Ru(II)-arene complex [RuCp(adeninate-κN7)(PPh_3)(PTA)] (PTA = 1,3,5-triaza-7-phosphaadamantane) was obtained and its antiproliferative activity was also analyzed. This complex displayed results comparable to those of cisplatin, and better than those of the deprotonated guanine derivative [21].

Herein we report a novel dinuclear Ru^{III} complex of formula [{Ru(μ-Cl)(μ-Hade)}$_2$Cl$_4$]$Cl_2\cdot 2H_2O$ (**1**) (Hade = protonated adenine). **1** is the first dinuclear ruthenium(III) system based on adenine. In this work, we discuss its preparation, crystal structure, electrochemical properties and anticancer activity.

2. Experimental

2.1. Materials

All starting chemicals and solvents used in the synthesis of **1** were purchased from commercial sources and used without further purification. Adenosine 5′-monophosphate (5′-AMP) (99.00%) was purchased from Acros Organics and the ruthenium precursor $K_2[RuCl_5(H_2O)]$ (99.95%) was acquired from Alfa Aesar.

2.2. Synthesis

2.2.1. Synthesis of [{Ru(μ-Cl)(μ-Hade)}$_2$Cl$_4$]$Cl_2\cdot 2H_2O$ (1)

A solvothermal reaction of $K_2[RuCl_5(H_2O)]$ (11.2 mg, 0.03 mmol) and adenosine 5′-monophosphate monohydrate (11.0 mg, 0.03 mmol) was carried out in HCl (4 mL, 3.0 M) at 90 °C for 3 days, followed by a 12 h cooling process to room temperature. Dark brown plates of **1** were thus grown and were suitable for X-ray diffraction studies. Yield: ca. 65%. Anal. Calcd. for $C_{10}H_{16}Cl_8N_8O_2Ru_2$: C, 15.1; H, 2.0; N, 17.6. Found: C, 15.2; H, 1.9; N, 17.7. SEM-EDX: a molar ratio of 1:4 for Ru/Cl was found for **1**. IR peaks (KBr pellets, ν/cm^{-1}): 3405(m), 3327(m), 3116(m), 3056(m), 2955(m), 2923(m), 2853(m), 1706(vs), 1653(m), 1616(m), 1559(m), 1521(w), 1466(s), 1404(m), 1320(m), 1234(s), 1180(m), 1135(m), 940(w), 800(w), 669(w), 608(m), 562(m), 414(w).

2.3. Physical measurements

Elemental analyses (C, H, N) and X-ray microanalysis were performed by the Central Service for the Support to Experimental Research (SCSIE) at the University of Valencia. The images and results of scanning electron microscopy (SEM-EDX) were obtained from a Hitachi S-4800 field emission scanning electron microscope, with 20 kV and 9.0 mm of accelerating voltage and working distance, respectively. Infrared spectrum (FT-IR) of **1** was recorded as a KBr pellet with a PerkinElmer Spectrum 65 FT-IR spectrometer in the range of 400 to 4000 cm^{-1} with 25 scans and a spectral resolution of 4 cm^{-1} (OMNIC 7.1a spectra software). Direct current (dc) magnetic susceptibility data were collected on a Quantum Design MPMS-XL SQUID magnetometer. The experimental magnetic data were corrected for the diamagnetic contributions of the constituent atoms as well as for the sample holder. Electrochemical studies were carried out on **1** by means of an Autolab/PGSTAT 204 scanning potentiostat operating at a scan rate range of 10–250 mV/s with Metrohm electrodes (NOVA 2.0 software). Cyclic voltammograms were performed by using 0.1 M $(NBu_4)[PF_6]$ as supporting electrolyte and a 10^{-3} M solution of **1** in dry *N*,*N*′-dimethylformamide (DMF). A glassy carbon disk of 0.32 cm^2 was used as working electrode, which was polished with 1.0 μm diamond powder, sonicated, washed with absolute ethanol and acetone, and air-dried. The AgCl/Ag reference electrode was separated from the test solution by a salt bridge containing the solvent/supporting electrolyte, with platinum as auxiliary electrode. All experiments were performed in standard electrochemical cells at 25 °C under argon. The investigated potential range was in the range of −1.5 to +1.5 *V* vs. AgCl/Ag. Ferrocene (Fc) was added as internal standard at the end of all the measurements.

Table 1
Crystal data and structure refinement for **1**.

Formula	$C_{10}H_{12}Cl_8N_{10}O_2Ru_2$
Formula weight	790.04
Crystal system	monoclinic
Space group	$P2_1/n$
Z	2
a (Å)	6.961(1)
b (Å)	19.042(2)
c (Å)	9.197(1)
α (°)	90
β (°)	101.20(1)
γ (°)	90
V(Å^3)	1195.9(2)
D_c (g cm^{-3})	2.194
F(000)	764.0
μ (mm^{-1})	2.189
Goodness-of-fit on F^2	1.175
R_1 [$I > 2\sigma(I)$][a] / all	0.0589 / 0.0719
wR_2 [b,c] / all	0.1630 / 0.1780

[a] $R_1 = \Sigma||F_o|-|F_c||/\Sigma|F_o|$.
[b] $wR_2 = \{\Sigma[w(F_o^2-F_c^2)^2]/[(w(F_o^2)^2]\}^{1/2}$.
[c] $w = 1/[\sigma^2(F_o^2) + (aP)^2 + bP]$ with $P = [F_o^2 + 2F_c^2]/3$.

2.4. Crystallographic data collection and structure determination

X-ray diffraction data collection from a single crystal of dimensions 0.16 × 0.06 × 0.02 mm^3 was performed on a Bruker D8 Venture diffractometer with graphite-monochromated Mo-K_α radiation (λ = 0.71073 Å). Crystal parameters and refinement results for **1** are summarized in Table 1. The structure of **1** was solved by standard direct methods and subsequently completed by Fourier recycling by using the SHELXTL software packages. The obtained model was refined with version 2017/1 of SHELXL against F^2 on all data by full-matrix least squares [22]. All non-hydrogen atoms were anisotropically refined, whereas the hydrogen atoms of the adenine molecule were set in calculated positions and refined isotropically by using the riding model. The hydrogen atoms of the water molecules were neither detected nor included into the model. The graphical manipulations were performed with DIAMOND program [23]. The CCDC code for **1** is 2.081.705.

2.5. Cancer cell line cultures

Two cancer cell lines from American Type Culture Collection (ATCC Rockville, MD) were used to test compound **1**: AGS (gastric cancer) and HCT116 (colon cancer). Cell lines were cultured following the conditions recommended by the supplier. The culture medium used in all cases was RPMI 1640 (Roswell Park Memorial Institute), supplemented with 10% Fetal Bovine Serum (GIBCO, New York, NY) and 1% Penicillin, under conditions of 37 °C at 5% CO_2.

2.6. Cell proliferation assays: MTT

Three thousand cells were cultured in 96-well plates during 24 h. After that, the cells were treated with 1, 10, 20 and 31 μM concentrations of **1** (the solvent being Polyethylene glycol 3350) in triplicate and the effect was measured at 48 and 72 h after treatment.

A 3-(4,5-dimethylthiazolyl-2)-2,5-diphenyltetrazolium bromide (MTT) assay was used to evaluate cell proliferation. MTT is a

colorimetric assay indicating cell survival and proliferation, which is based on the metabolic reduction of the MTT by the mitochondrial enzyme succinate dehydrogenase, under defined conditions, to a purple-coloured compound (formazan), thus allowing the determination of the mitochondrial function of the treated cells. MTT, a yellow tetrazole, is reduced to purple in living cells. A dimethyl sulfoxide (DMSO) solution is added to solubilize the compound and convert the insoluble purple formazan into a coloured solution, the absorbance of which is measured at 560 nm in the spectrophotometer. An increase in absorbance corresponds to an increase in cell proliferation, while a decrease in absorbance means a decrease in cell proliferation. Each value is repeated in triplicate and the mean is calculated. Each absorbance of the tested compound is checked with its respective untreated control. Viability is calculated according to the following equation: % Viability = (Optical Density treated cells x 100) / Optical Density control cells.

2.7. Apoptosis evaluation by cytometry

Three thousand cells were cultured in 96-well plates during 24 h. After that, the cells were treated with 1, 10, 20 and 31 μM of compound **1** in triplicate, and the effect was measured at 48 and 72 h after treatment.

Cells were washed with cold phosphate buffered saline (PBS) and trypsinized with 0.05% trypsin and the collected cells were then centrifuged at 1500 rpm at 4 °C for 5 min.

The pellet collection was staining for Annexin *V*-FITC and phycoerythrin-Cyanine7 (PE-Cy7)-A using an apoptosis detection kit II (Pharmingen, San Diego, CA, USA) based on the binding properties of annexin A5 to phosphatidylserine with a vital dye such as propidium iodide (PI). Samples were diluted in binding buffer. From this solution and aliquot of 100 mL was stained with 5 mL Protein A conjugated with fluorescein isothiocyanate (A-FITC) solution and 10 mL PI solution. Samples were incubated for 15 min, and 400 mL of binding buffer was added. Samples were analyzed within 1 h. The samples were analyzed using a BD FACSVERSE Cell Analyzer (BD Bioscience) equipped with standard optics. An Ar-ion laser (INNOVA 90, Coherent, Santa Clara, CA, USA) tuned at 488 nm and running at 200 mW was used as light source. From each cell, forward light scatter (FSC), orthogonal light scatter (SSC), A-FITC fluorescence, and PI fluorescence were evaluated using Cellquest version 3.3 (Becton Dickinson, San Jose, CA, USA). The percentages of Annexin-*V* negative or positive, and PI negative or positive as well as double positive cells were evaluated, based on quadrants determined from single-stained and unstained control samples.

3. Results and discussion

3.1. Synthetic procedure

By reacting the ruthenium(III) precursor $K_2[RuCl_5(H_2O)]$ with adenine 5′-monophosphate (5′-AMP) in a hydrochloric acid (3.0 M) solution, we prepared a novel purine-based ruthenium(III) complex of formula $[\{Ru(\mu\text{-}Cl)(\mu\text{-}Hade)\}_2Cl_4]Cl_2{\cdot}2H_2O$ (**1**). The synthetic procedure was performed by heating the reaction mixture at 90 °C through a solvothermal method. As crystallization technique, the process continued during a further 12 h cooling step to room temperature. In this way, dark brown crystals of **1** were obtained in satisfactory yield (65%). The nucleotide 5′-AMP was used here as starting material of **1** because it is a suitable source of adenine. Besides, a better yield was obtained when 5′-AMP was employed instead of just adenine. To obtain compound **1** the combination of the solvothermal method and strong acid medium is mandatory, leading to the hydrolysis of the nucleotide precursor and the protonation of the adenine moiety at N1 atom. These results support the fact that this is an adequate synthetic method to obtain purine-based diruthenium(III) compounds [24].

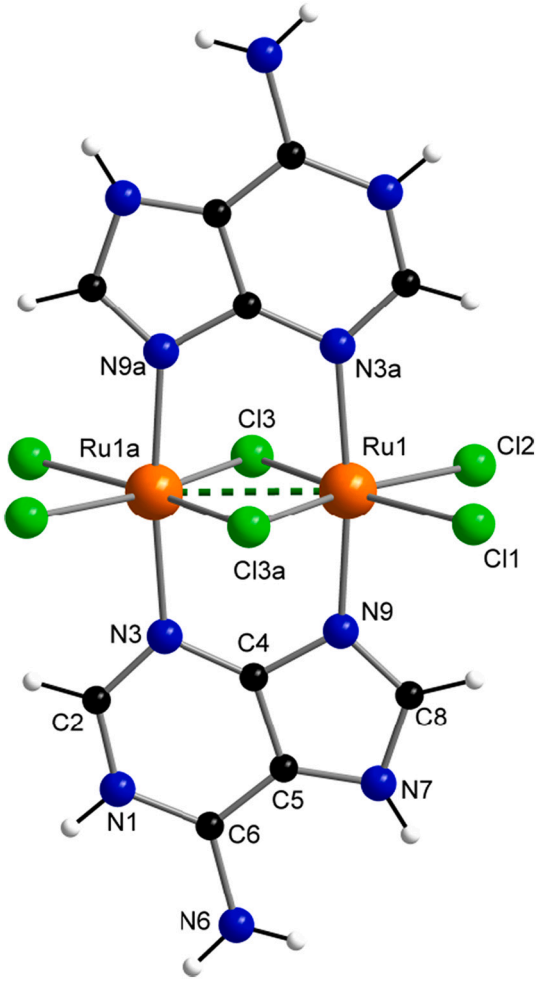

Fig. 1. Molecular structure of the $[\{Ru(\mu\text{-}Cl)(\mu\text{-}Hade)\}_2Cl_4]^{2+}$ complex in **1** along with the atom labels scheme.

3.2. Crystal structure of $[\{Ru(\mu\text{-}Cl)(\mu\text{-}Hade)\}_2Cl_4]Cl_2{\cdot}2H_2O$ (1)

The crystal structure of **1** was obtained by single-crystal X-ray diffraction. A Cambridge Structural Database (CSD) survey revealed that **1** is the first reported compound with a crystal structure based on a dinuclear Ru(III) compound containing adenine. **1** crystallizes in the monoclinic system, with space group $P2_1/n$ (Table 1), and its core is very similar to that of the previously reported neutral $[\{Ru(\mu\text{-}Cl)(\mu\text{-}hpx)\}_2Cl_4]$ (hpx = hypoxanthine molecule) complex, which crystallizes in the monoclinic system with space group $P2_1/c$ [24]. The crystal structure of **1** is made up of dinuclear cationic $[\{Ru(\mu\text{-}Cl)(\mu\text{-}Hade)\}_2Cl_4]^{2+}$ complexes, chloride anions and H_2O molecules. The asymmetric unit of **1** consists of half a $[\{Ru(\mu\text{-}Cl)(\mu\text{-}Hade)\}_2Cl_4]^{2+}$ complex, one chloride and one water molecule (Fig. 1).

Each Ru(III) ion is bonded to four chloride ions and two nitrogen atoms (N3 and N9) from two purine bases in a distorted octahedral environment, the N1 being protonated in both adenine molecules. The two Ru(III) ions are connected each other through two adenine molecules and two chloro-bridges (Fig. 1). In **1**, a very short intramolecular Ru···Ru distance [Ru(1)···Ru(1a) = 2.713 Å, (a) = −x + 1, −y + 1, −z + 2] indicates the formation of a metal-metal bond (dashed lines in Fig. 1). The average values of the Ru—Cl [2.329(1) Å] and Ru—N [2.067(1) Å] bond lengths are in agreement with those values found in the literature for previously reported Ru(III) complexes with a similar environment [24,25]. The adenine molecules in **1** show C—C and C—N bond lengths with values which are in agreement with those previously reported for

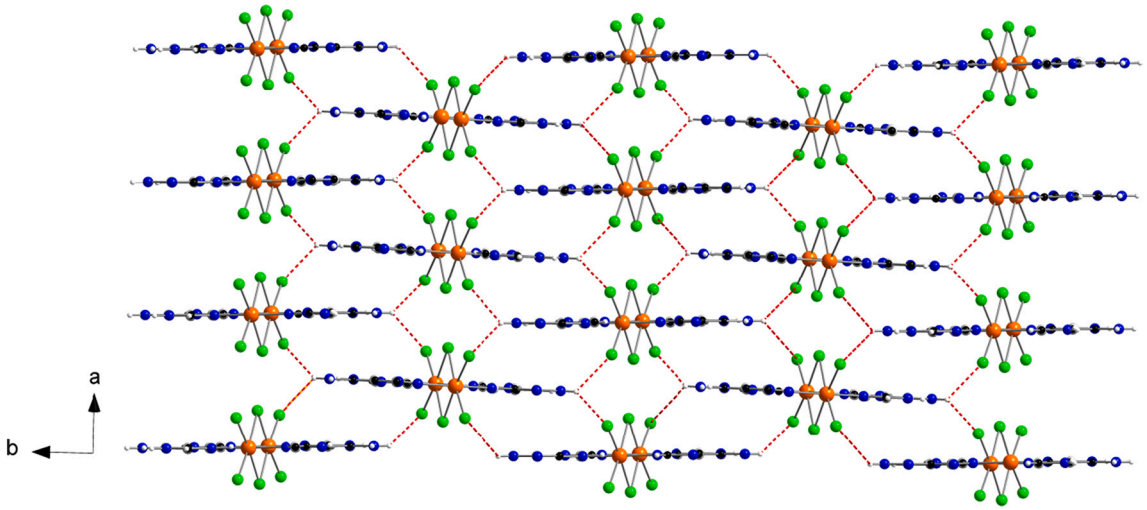

Fig. 2. View along the crystallographic *c* axis of a fragment of the crystal packing of **1**. H-bonding interactions between Cl^- anions and N—H groups of adjacent $[\{Ru(\mu\text{-}Cl)(\mu\text{-}Hade)\}_2Cl_4]^{2+}$ units are shown as red-dashed lines. Non-coordinating Cl^- anions and water molecules have been omitted for clarity. (For interpretation of the references to colour in this figure legend, the reader is referred to the web version of this article.)

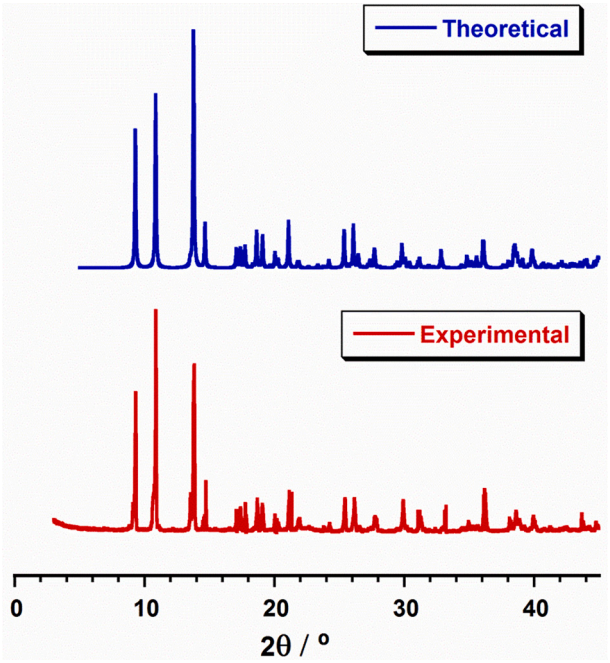

Fig. 3. Plot of the experimental (red) and theoretical (blue) powder X-ray diffraction (PXRD) patterns profile (2θ/°) in the range 0–45° for **1**. (For interpretation of the references to colour in this figure legend, the reader is referred to the web version of this article.)

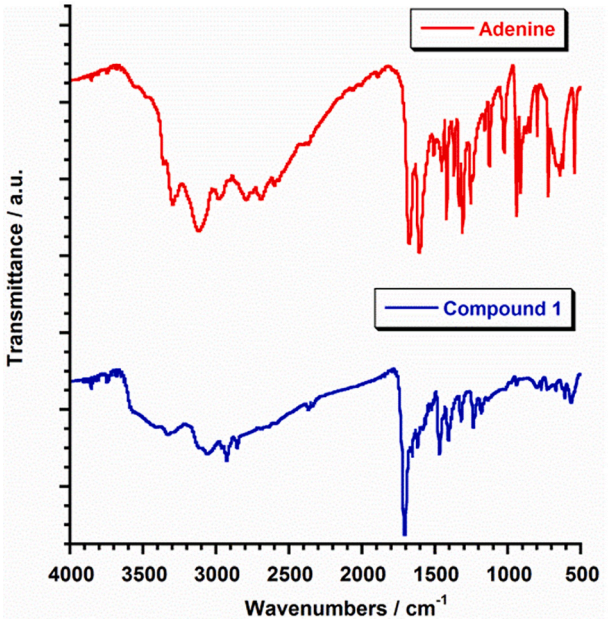

Fig. 4. FT-IR spectra for adenine (red) and compound **1** (blue), see text. (For interpretation of the references to colour in this figure legend, the reader is referred to the web version of this article.)

compounds containing this nucleobase [26–33].

In the crystal packing of **1**, the $[\{Ru(\mu\text{-}Cl)(\mu\text{-}Hade)\}_2Cl_4]^{2+}$ cations and Cl^- anions are arranged in an alternate way. The shortest intermolecular Cl···Cl interaction of ca. 3.373(2) Å connects the $[\{Ru(\mu\text{-}Cl)(\mu\text{-}Hade)\}_2Cl_4]^{2+}$ units each other generating chains that grow along the crystallographic *a* axis [Cl(3)···Cl(3b), (b) = −x, −y + 2, −z + 2] (Fig. 2). H-bonding interactions between Cl^- anions and N—H groups of adjacent $[\{Ru(\mu\text{-}Cl)(\mu\text{-}Hade)\}_2Cl_4]^{2+}$ units [with Cl···N separations of ca. 3.193(3) Å] lead these chains to the formation of a two-dimensional network, which is extended along the *ab* plane (Fig. 2). The shortest intermolecular Ru···Ru distance is ca. 6.76 Å [Ru(1)···Ru(1c), (c) = −x + 1, −y + 2, −z + 1]. Although no π···π interactions are observed in **1** [the shortest centroid···centroid distance being approximately 5.701(1) Å], Cl···π interactions of approximately 3.501(1) Å take place between intercalated Cl^- anions and the pyrimidine ring of adenine molecules. The supramolecular network is supported by additional H-bonding interactions, which stabilize the crystal structure in **1**. The powder X-ray diffraction (PXRD) pattern of **1** confirmed the homogeneity of the bulk sample (Fig. 3).

3.3. Infrared spectroscopy

The infrared (IR) spectrum of **1** along with that of the free adenine ligand are given in Fig. 4. The IR spectrum of adenine has been previously studied [34,35], so that it has been added in this work only for comparison. In general, the vibrational bands mainly associated to the N—H symmetric (ν_s) and asymmetric (ν_{as}) stretching for the free adenine molecule were more intense and complex that those of **1** in the ca.

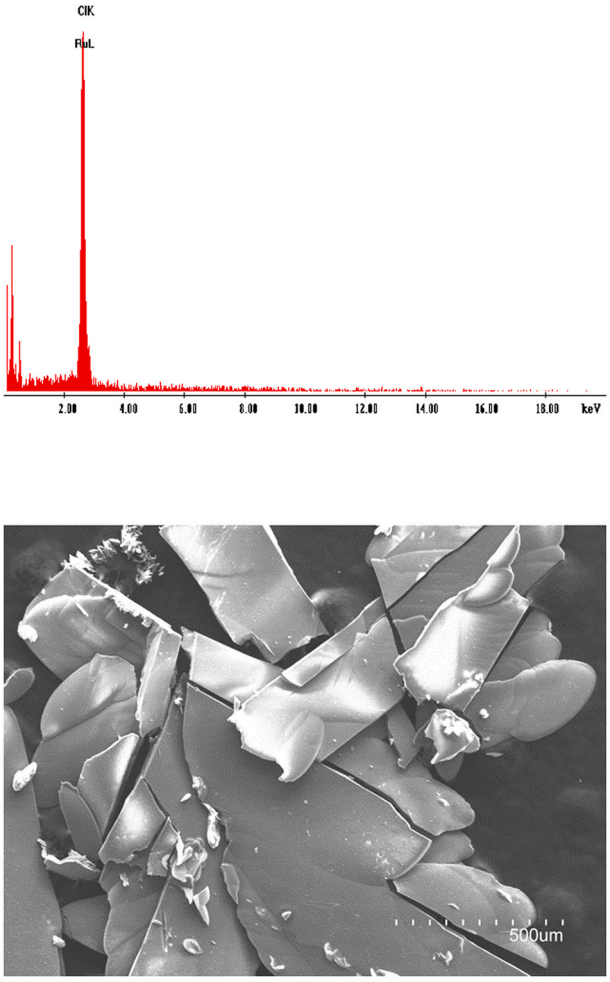

Fig. 5. (Top) Energy dispersive X-ray analysis (EDX) spectrum for **1**. (Bottom) Scanning electron microscopy (SEM) image of crystals of **1**.

3800–2000 cm^{-1} region (Fig. 4), which would be due to a more ordered hydrogen-bonding network in the crystalline solid for the free ligand [34,35]. The experimental $\nu_{as}(NH_2)$ value of the adenine molecule observed at 3296 cm^{-1} was slightly shifted to higher wavenumbers when compared with that detected for **1** [3327 cm^{-1}], whereas the experimental $\nu_s(NH_2)$ value remained pretty much unaltered in the IR spectrum of **1** [3116 cm^{-1}] (Fig. 4). In the 1800–500 cm^{-1} region, the most interesting features were the two strong vibrational bands associated to the stretching ν(C=N) and ν(C=C) and bending $\delta(NH_2)$, mainly scissoring, which were found at 1680 and 1600 cm^{-1} for the adenine molecule [34,35]. These vibrational bands were transformed into only one band, which was observed at 1706 cm^{-1} for **1**, with this fact indicating the coordination of the Ru^{III} metal ions to adenine molecules in compound **1** (Fig. 4). The Ru—Cl band is expected to be found around 310–330 cm^{-1}. Unfortunately, we cannot report this value for compound **1** given that our IR device works in the 4000–400 cm^{-1} range.

3.4. Scanning electron microscopy - energy dispersive X-ray analysis

A sample of compound **1** was measured through of scanning electron microscopy and energy dispersive X-ray analysis (SEM-EDX), these analyses being carried out as previously performed for other ruthenium systems [36,37]. The results of the microanalysis gave a Ru/Cl molar ratio of 1:4. An example of the recorded images of **1** is given in Fig. 5, where crystals of **1** are shown as plates.

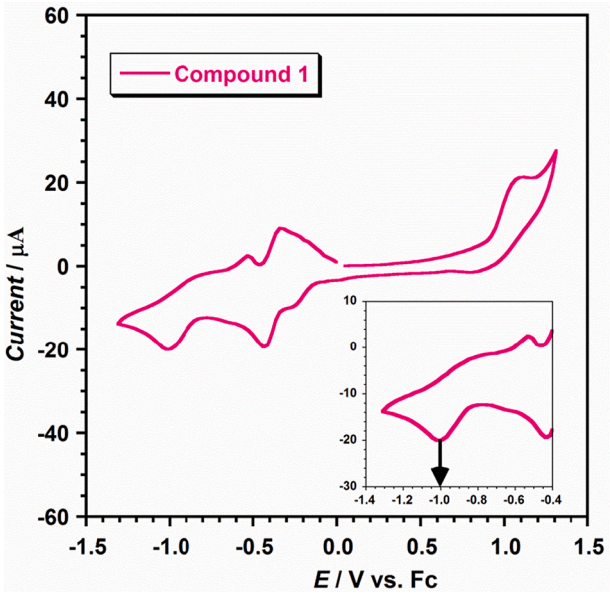

Fig. 6. Cyclic voltammogram of **1** in a dry DMF 10^{-3} M solution with 0.1 M $(NBu_4)[PF_6]$ at 25 °C and scan rate 200 m*V*/s. The area of the working electrode is 0.32 cm^2. The inset shows a detail of reduction peak assigned to adenine.

3.5. Magnetic properties

Direct current (dc) magnetic susceptibility measurements were carried out on a microcrystalline sample of compound **1** and under an external magnetic field of 1000 G. These measurements revealed that **1** is diamagnetic at room temperature. The value of its molar magnetic susceptibility (χ_M) was calculated to be −0.0296 cm^3mol^{-1} at 300 K. The diamagnetic nature observed for **1** is mainly due to a very strong antiferromagnetic coupling between the involved ruthenium ions ($4d^5$ configuration and $S = 1/2$ each), that are connected through two adeninium ligands and two chloro bridges, which lead to the formation of a metal-metal bond and hence generating a ruthenium system with $S = 0$.

3.6. Electrochemical properties

The electrochemical properties of **1** were investigated by means of cyclic voltammetry (CV) in dry *N*,*N*′-dimethylformamide (DMF), containing 0.1 M $(NBu_4)[PF_6]$, in the range of potential between +1.5 and − 1.5 *V* and at room temperature. The CV plot obtained is shown in Fig. 6.

Dinuclear ruthenium compounds containing metal–metal bonds have been studied for several decades [38]. They show electronic structures and redox properties which are strongly depending on the solvent and the supporting electrolyte and, in general, are well-known [39–41]. Therefore, this type of Ru—Ru compounds could be an acceptable reference in electrochemical studies applied in several areas of investigation [39–41]. In the CV curves of **1**, three reduction processes can be observed (Fig. 6). The first two reduction peaks were found between 0.0 V and − 0.50 V, which would be associated to the formation of the mixed-valent Ru(II)-Ru(III) species [at −0.27 V] and also to that of the Ru(II)-Ru(II) system [at −0.43 V]. These reduction potential values are very close to those reported for similar diruthenium compounds [39–41]. Nevertheless, much more interesting would be the third detected reduction peak, which would be generated by the influence of the adenine ligand and would be observed at −1.00 *V*, see inset in Fig. 6. It is worth mention that this value assigned to adenine is in agreement with those previously reported for this purine nucleobase in electrochemistry studies performed through modified electrodes based on different polianiline-MnO_2 [42] and graphite-WS_2 composite materials

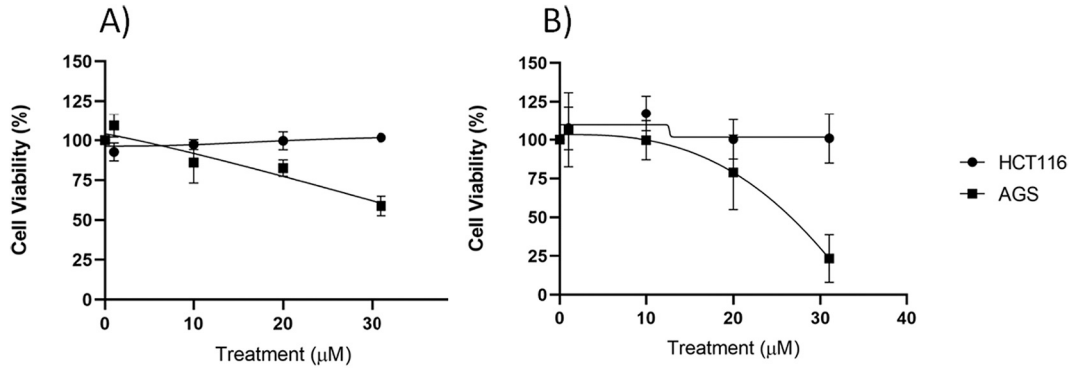

Fig. 7. Cell viability obtained by MTT assay. Cells were seeded in 12-well plates at a density of 3×10^3 cells/mL and allowed to grow for 24 h before treatments. Concentrations: 1, 10, 20 and 31 μM. Treatment duration was performed at 48 (A) and 72 h (B). Cell viability was determined by MTT assay at each time point, including the baseline and the DMSO (1:1000), and for each treatment. The method was carried out at least three times in triplicate.

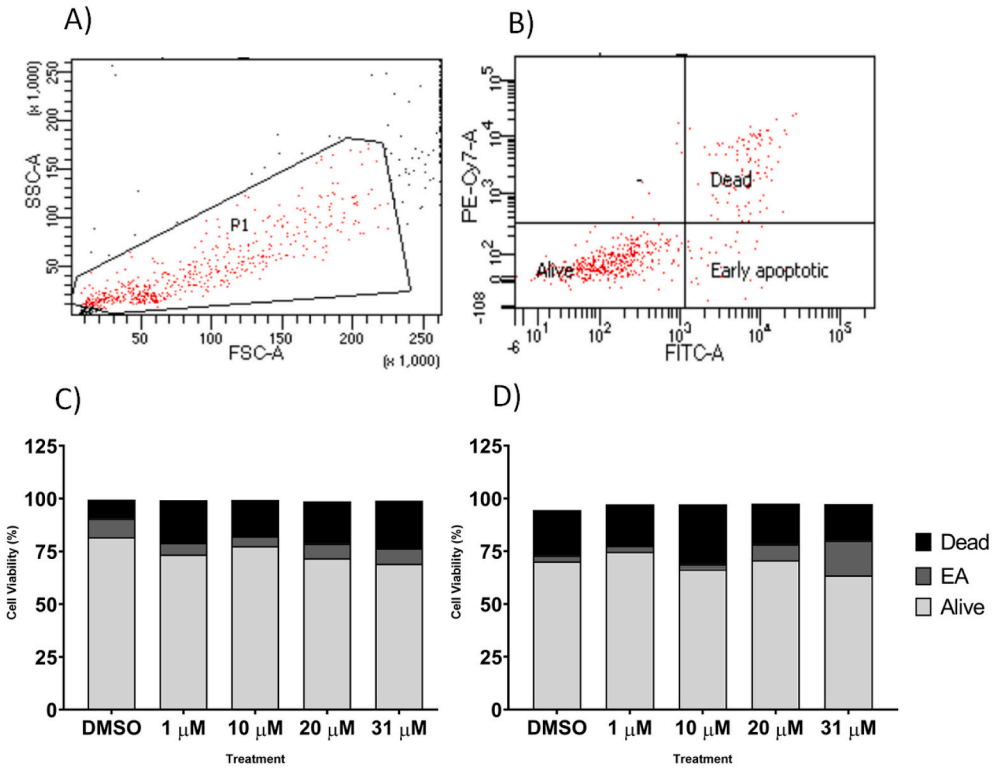

Fig. 8. (A) Cells events were selected from debris against forward (FSC-A) and side (SSC-A) scatter parameters. (B) Dot plot of gated cells staining with Annexin-V (FITC-A) and iodine propidium (PE-Cy7-A) in AGS cell lines. The upper right quadrant represents necrotic cells binding Annexin-V and PI, the lower right quadrant shows early apoptotic cells which bind Annexin-V but exclude PI, alive cells are represented in the lower left quadrant with no signal from Annexin-V neither from PI. Piled histogram representing the proportion of alive (light grey), necrotic cells (black) and early apoptotic (EA) cells (dark grey) in (C) HTC116 cells and (D) AGS cells at 48 h and at different concentrations of **1**.

[43], which shown high accuracy and promising redox activity toward purine nucleobases [42,43]. In addition, a similar electrochemical behavior was observed in the case of the hypoxanthine molecule when linked to this type of diruthenium compound, with a reduction peak for this other purine found at −0.82 V [24]. In order to analyze the repeatability of the CV curves they were measured for five times. Indeed, a relative standard deviation value of approximately 1.4% for the current response was obtained for **1**. This latter fact shows the reliability and stability achieved by this type of diruthenium compounds [44].

3.7. Viability of AGS and HCT116 cells treated with *1*

Cytotoxicity of **1** was analyzed in HCT116 and AGS cell lines by MTT assay and cell cytometry. The cell lines were subjected to increasing concentrations of **1** (1, 10, 20 and 31 μM) for 48 and 72 h. As shown in Fig. 7A, it is observed a small dose-time-dependent reduction in cell proliferation when **1** is tested in the AGS cell lines and 48 h incubation at 10 and 20 μM concentrations. However, MTT assay showed 42% viability reduction at 31 μM (Fig. 7A). Again, when MTT assay was performed at 72 h incubation a strong reduction of more than 90% viability can be detected at 31 μM (Fig. 7B). Therefore, IC_{50} for **1** was detected at 23.25 μM when 72 h incubation were tested. In addition, our results showed that compound **1** displays low to none activity against HCT116 cells. In Fig. 8, a small increase of early apoptotic cells can be seen at the highest concentration (31 μM) of **1**.

4. Conclusions

A novel dinuclear ruthenium(III) complex of formula [{Ru(μ-Cl)(μ-Hade)}$_2$Cl$_4$]Cl$_2$·2H$_2$O (**1**) was synthesized by reacting the precursor K$_2$[RuCl$_5$(H$_2$O)] with adenine 5′-monophosphate (5′-AMP) in a hydrochloric acid solution. **1** is the first dinuclear ruthenium(III) system based on adenine. This adenine-based diruthenium complex was characterized through Fourier transform infrared spectroscopy (FT–IR), scanning

electron microscopy, energy dispersive X-ray analysis (SEM–EDX), magnetometer (SQUID) and single-crystal X-ray diffraction. The study of its electrochemical properties by means of cyclic voltammetry (CV) technique revealed a behavior typical of dinuclear Ru(III) compounds containing a metal–metal bond, displaying a well-resolved reduction peak assignable to the adenine molecule.

Compound **1** has only shown anticancer activity on gastric cancer cells (AGS), by inducing apoptosis at the highest concentration. Cisplatin is one of the most active drugs for cancer treatment, but also a high toxicity inducer. In comparison, cisplatin has been tested in AGS cell lines of gastric origin detecting anticancer activities at IC_{50} of 4.84 μM and 16.6 μM [45,46]. Our results obtained with **1** show higher IC_{50} (but in a similar range of molarity) than those previously published with the same cell line being treated with cisplatin. In our study, the drug activity was not tested on normal cell lines for comparison. Nevertheless, we have used a negative control group using the cell lines treated with the vehicle compound without the chemotherapy drug in each experiment. In any case, this is the first time that a dinuclear ruthenium (III) complex based on adenine has been tested toward cancer cell lines, and further studies will be performed to get new insights into its potential chemotherapeutic action.

Ethical approval

Not required.

Data availability statement

The raw data that support the findings of this study are available from the corresponding author upon reasonable request.

Declaration of Competing Interest

The authors declare that they have no known competing financial interests or personal relationships that could have appeared to influence the work reported in this paper.

Acknowledgements

This research was funded by the VLC-BIOCLINIC Program of the University of Valencia [Projects 02-RUN-AT-MARTINEZ-RIBAS-2017-A and PI-2021-007-DIRUGEN] and the Spanish Ministry of Science and Innovation [Projects PID2019-109735GB-I00 and CEX2019-000919-M (*Excellence Unit "María de Maeztu"*)].

Appendix A. Supplementary data

Supplementary data to this article can be found online at https://doi.org/10.1016/j.jinorgbio.2022.111812.

References

[1] S. Higgins, Regarding ruthenium, Nature Chem. 2 (2010) 1100.
[2] C. Bruneau, M. Achard, Allylic ruthenium(IV) complexes in catalysis, Coord. Chem. Rev. 256 (2012) 525–536.
[3] L. Duan, F. Bozoglian, S. Mandal, B. Stewart, T. Privalov, A. Llobet, L. Sun, A molecular ruthenium catalyst with water-oxidation activity comparable to that of photosystem II, Nature Chem. 4 (2012) 418–423.
[4] T. Friedberger, J.W. Ziller, Z. Guan, Ruthenium(IV) complexes for ethylene insertion polymerization, Organometallics 33 (2014) 1913–1916.
[5] Z. Adhireksan, G.E. Davey, P. Campomanes, M. Groessl, C.M. Clavel, H. Yu, A. A. Nazarov, C.H.F. Yeo, W.H. Ang, P. Dröge, U. Rothlisberger, P.J. Dyson, C. A. Davey, Ligand substitutions between ruthenium–cymene compounds can control protein versus DNA targeting and anticancer activity, Nat. Commun. 5 (2014) 3462.
[6] Y. Yamamoto, Y. Tamaki, T. Yui, K. Koike, O. Ishitani, New Light-Harvesting Molecular Systems Constructed with a Ru(II) Complex and a Linear-Shaped Re(I) Oligomer, J. Am. Chem. Soc. 132 (2010) 11743–11752.
[7] J. Ferrando-Soria, J. Vallejo, M. Castellano, J. Martínez-Lillo, E. Pardo, J. Cano, I. Castro, F. Lloret, R. Ruiz-García, M. Julve, Molecular magnetism, quo vadis? A historical perspective from a coordination chemist viewpoint, Coord. Chem. Rev. 339 (2017) 17–103.
[8] M.J. Clarke, Ruthenium metallopharmaceuticals, Coord. Chem. Rev. 236 (2003) 209–233.
[9] C. Mari, V. Pierroz, S. Ferrari, G. Gasser, Combination of Ru(II) complexes and light: new frontiers in cancer therapy, Chem. Sci. 6 (2015) 2660–2686.
[10] S.P. Mulcahy, K. Gründler, C. Frias, L. Wagner, A. Prokop, E. Meggers, Discovery of a strongly apoptotic ruthenium complex through combinatorial coordination chemistry, Dalton Trans. 39 (2010) 8177–8182.
[11] L. Zeng, P. Gupta, Y. Chen, E. Wang, L. Ji, H. Chao, Z.-S. Chen, The development of anticancer ruthenium(II) complexes: from single molecule compounds to nanomaterials, Chem. Soc. Rev. 46 (2017) 5771–5804.
[12] F. Li, J.G. Collins, F.R. Keene, Ruthenium complexes as antimicrobial agents, Chem. Soc. Rev. 44 (2015) 2529–2542.
[13] D. Musumeci, L. Rozza, A. Merlino, L. Paduano, T. Marzo, L. Massai, L. Messori, D. Montesarchio, Interaction of anticancer Ru(III) complexes with single stranded and duplex DNA model systems, Dalton Trans. 44 (2015) 13914–13925.
[14] J. Furrer, G. Süss-Fink, Thiolato-bridged dinuclear arene ruthenium complexes and their potential as anticancer drugs, Coord. Chem. Rev. 309 (2016) 36–50.
[15] C.G. Hartinger, S. Zorbas-Seifried, M.A. Jakupec, B. Kynast, H. Zorbas, B. K. Keppler, From bench to bedside – preclinical and early clinical development of the anticancer agent indazolium trans-[tetrachlorobis(1H-indazole)ruthenate(III)] (KP1019 or FFC14A), J. Inorg. Biochem. 100 (2006) 891–904.
[16] C.G. Hartinger, M.A. Jakupec, S. Zorbas-Seifried, M. Groessl, A. Egger, W. Berger, H. Zorbas, P.J. Dyson, B.K. Keppler, KP1019, a new redox-active anticancer agent – preclinical development and results of a clinical phase I study in tumor patients, Chem. Biodivers. 5 (2008) 2140–2155.
[17] W.H. Ang, A. Casini, G. Sava, P.J. Dyson, Organometallic ruthenium-based antitumor compounds with novel modes of action, J. Organomet. Chem. 696 (2011) 989–998.
[18] R.S. Correa, V. Freire, M.I.F. Barbosa, D.P. Bezerra, L.M. Bomfim, D.R.M. Moreira, M.B.P. Soares, J. Ellena, A.A. Batista, Ru(II)–thyminate complexes: New metallodrug candidates against tumor cells, New J. Chem. 42 (2018) 6794–6802.
[19] S.L.R. Silva, I.R.S. Baliza, R.B. Dias, C.B.S. Sales, C.A.G. Rocha, M.B.P. Soares, R. S. Correa, A.A. Batista, D.P. Bezerra, Ru(II)-thymine complex causes DNA damage and apoptotic cell death in human colon carcinoma HCT116 cells mediated by JNK/p38/ERK1/2 via a p53-independent signaling, Sci. Rep. 9 (2019) 11094.
[20] I. Turel, M. Pečanac, A. Golobič, E. Alessio, B. Serli, A. Bergamo, G. Sava, Solution, solid state and biological characterization of ruthenium(III)-DMSO complexes with purine base derivatives, J. Inorg. Biochem. 98 (2004) 393–401.
[21] L. Hajji, C. Saraiba-Bello, G. Segovia-Torrente, F. Scalambra, A. Romerosa, CpRu complexes containing water soluble phosphane PTA and natural purines adenine, guanine and theophylline: synthesis, characterization, and antiproliferative properties, Eur. J. Inorg. Chem. 38 (2019) 4078–4086.
[22] Bruker Analytical X-ray Instruments. SHELXL-2017/1; Bruker Analytical X-ray Instruments: Madison, WI, USA, 2017.
[23] DIAMOND 4.5.0. Crystal Impact GbR: Bonn, Germany, 2018.
[24] M. Orts-Arroyo, I. Castro, J. Martínez-Lillo, Detection of Hypoxanthine from inosine and unusual hydrolysis of immunosuppressive drug azathioprine through the formation of a diruthenium(III) system, Biosensors 11 (2021) 19.
[25] D. Armentano, J. Martínez-Lillo, Hexachlororhenate(IV) salts of ruthenium(III) cations: X-ray structure and magnetic properties, Inorg. Chim. Acta 380 (2012) 118–124.
[26] C. Gagnon, J. Hubert, R. Rivest, A.L. Beauchamp, Crystal structure of di-μ-adeninium-disilver(I) perchlorate monohydrate, Inorg. Chem. 16 (1977) 2469–2473.
[27] C.H. Wei, K.B. Jacobson, X-ray crystallographic characterization of an adenine-cadmium(II) complex, di-μ-adeninium-di-μ-aquo-tetrakis(nitrato-O,O')dicadmium (II) dinitrate, containing a cationic nucleic acid base as a bidentate ligand, Inorg. Chem. 20 (1981) 356–363.
[28] A.K. Mishra, R.K. Prajapati, S. Verma, Probing structural consequences of N9-alkylation in silver-adenine frameworks, Dalton Trans. 39 (2010) 10034–10037.
[29] Y. Song, X. Yin, B. Tu, Q. Pang, H. Li, X. Ren, B. Wang, Q. Li, Metal–organic frameworks constructed from mixed infinite inorganic units and adenine, CrystEngComm 16 (2014) 3082–3085.
[30] D. Armentano, M.A. Barquero, C. Rojas-Dotti, N. Moliner, G. De Munno, E. K. Brechin, J. Martínez-Lillo, Enhancement of Intermolecular Magnetic Exchange through Halogen···Halogen Interactions in Bisadeninium Rhenium(IV) Salts, Cryst. Growth Des. 17 (2017) 5342–5348.
[31] Hui-Fang Ma, Li-Wen Ding, Lin Chen, Yu-Ling Wang, Qing-Yan Liu, Two cadmium compounds with adenine and carboxylate ligands: syntheses, structures and photoluminescence, J. Coord. Chem. 70 (2017) 145–155.
[32] A. Valentín-Pérez, J. Perles, S. Herrero, R. Jiménez-Aparicio, Coordination capacity of cytosine, adenine and derivatives towards open-paddlewheel diruthenium compounds, J. Inorg. Biochem. 187 (2018) 109–115.
[33] J. Pascual-Colino, G. Beobide, O. Castillo, P. Lodewyckx, A. Luque, S. Pérez-Yáñez, P. Román, L.F. Velasco, Adenine nucleobase directed supramolecular architectures based on ferrimagnetic heptanuclear copper(II) entities and benzenecarboxylate anions, J. Inorg. Biochem. 202 (2020) 110865.
[34] G.C.P. Van Zundert, S. Jaeqx, G. Berden, J.M. Bakker, K. Kleinermanns, J. Oomens, A.M. Rijs, IR spectroscopy of isolated neutral and protonated adenine and 9-methyladenine, ChemPhysChem 12 (2011) 1921–1927.
[35] K.B. Beć, J. Grabska, M.A. Czarnecki, W. Huck, M.J. Wójcik, T. Nakajima, Y. Ozaki, IR spectra of crystalline nucleobases: combination of periodic harmonic calculations with anharmonic corrections based on finite models, J. Phys. Chem. B 123 (2019) 10001–10013.

[36] S.S. Mohite, A.B. Patil-Deshmukh, S.S. Chavan, Synthesis and characterization of Ru(III) complexes with 2-(E)-((4-((4-bromophenyl)ethynyl)phenyl)imino)methyl-4-((E)-phenyldiazenyl)phenol and their use as a precursor for RuO_2 nanoparticles, J. Mol. Struct. 1176 (2019) 386–393.
[37] V.P. Sur, A. Mazumdar, P. Kopel, S. Mukherjee, P. Vítek, H. Michalkova, M. Vaculovičová, A. Moulick, A novel ruthenium based coordination compound against pathogenic bacteria, Int. J. Mol. Sci. 21 (2020) 2656.
[38] F.A. Cotton, E. Pedersen, Magnetic and electrochemical properties of transition metal complexes with multiple metal-to-metal bonds. II. Tetrabutyratodiruthenium (n+) with n = 0 and 1, Inorg. Chem. 14 (1975) 388–391.
[39] T. Malinski, D. Chang, F.N. Feldmann, J.L. Bear, K.M. Kadish, Electrochemical studies of a novel ruthenium(II,III) dimer, trifluoroacetamidatoruthenium chloride ($Ru_2(HNOCCF_3)_4Cl$), Inorg. Chem. 22 (1983) 3225–3233.
[40] Y. Hiraoka, T. Ikeue, H. Sakiyama, F. Guégan, D. Luneau, B. Gillon, I. Hiromitsu, D. Yoshioka, M. Mikuriya, Y. Kataoka, M. Handa, An unprecedented up-field shift in the ^{13}C NMR spectrum of the carboxyl carbons of the lantern-type dinuclear complex TBA[$Ru_2(O_2CCH_3)_4Cl_2$] (TBA^+ = tetra(n-butyl)ammonium cation), Dalton Trans. 44 (2015) 13439–13443.
[41] Y. Kataoka, S. Mikami, H. Sakiyama, M. Mitsumi, T. Kawamoto, M. Handa, A neutral paddlewheel-type diruthenium(III) complex with benzamidinato ligands: Synthesis, crystal structure, magnetism, and electrochemical and absorption properties, Polyhedron 136 (2017) 87–92.
[42] M.U.A. Prathap, R. Srivastava, B. Satpati, Simultaneous detection of guanine, adenine, thymine, and cytosine at polyaniline/MnO_2 modified electrode, Electrochim. Acta 114 (2013) 285–295.
[43] J. Zhang, D. Han, S. Wang, X. Zhang, R. Yang, Y. Ji, X. Yu, Electrochemical detection of adenine and guanine using a three-dimensional WS_2 nanosheet/graphite microfiber hybrid electrode, Electrochem. Commun. 99 (2019) 75–80.
[44] M. Orts-Arroyo, I. Castro, F. Lloret, J. Martínez-Lillo, Molecular self-assembly in a family of oxo-bridged dinuclear ruthenium(IV) systems, Cryst. Growth Des. 20 (2020) 2044–2056.
[45] S.A. Suttie, K.G.M. Park, T.A.D. Smith, [^{18}F]2-Fluoro-2-deoxy-D-glucose incorporation by AGS gastric adenocarcinoma cells in vitro during response to epirubicin, cisplatin and 5-fluorouracil, Br. J. Cancer 97 (2007) 902–909.
[46] B. Mora-Lagos, I. Cartas-Espinel, I. Riquelme, A.C. Parker, S.R. Piccolo, T. Viscarra, Functional and transcriptomic characterization of cisplatin-resistant AGS and MKN-28 gastric cancer cell lines, PLOS ONE 15 (1) (2020) e0228331.